Decadal Shift in the Relationship between Winter Arctic Oscillation and Central Indian Ocean Precipitation during the Early 2000s

Yiwen SHI[1,2,3], Yi CHEN[1,2,3], and Daoyi GONG[1,2,3*]

1 *Key Laboratory of Environmental Change and Natural Disaster of Ministry of Education*, *Beijing Normal University*, *Beijing* 100875
2 *Academy of Disaster Reduction and Emergency Management*, *Faculty of Geographical Science*, *Beijing Normal University*, *Beijing* 100875
3 *State Key Laboratory of Earth Surface Processes and Resource Ecology*, *Beijing Normal University*, *Beijing* 100875

(Received January 15, 2021; in final form July 5, 2021)

ABSTRACT

The present study investigated the long-term change in the interannual relationship between the boreal winter Arctic Oscillation (AO) and tropical Indian Ocean (TIO) climate during 1979–2019 and found that their linkage experienced a decadal change in 2001/2002. The 19-yr sliding correlation coefficient between the January–February–March (JFM) AO index and central TIO (0–10°S, 65°–80°E) precipitation was significant, with values of approximately 0.50–0.75 during 1979–2001, but abruptly decreased to 0.35 in 2002 and 0.10 in 2010. Meanwhile, the spatial patterns of the AO-related atmospheric circulation anomalies also displayed different features before and after 2001. During 2002–2019, the anomalous anticyclone in the middle troposphere over the Arabian Sea moved northwestward and strengthened, and the JFM AO was more closely correlated to the anticyclone, with correlation coefficient changed from −0.38 before 2001 to −0.63 after 2001; correspondingly, strong cross-equator air flows were observed over the western TIO (40°–50°E), but no significant anomalies of precipitation in the central TIO were observed. During 1979–2001, however, significant southward cross-equator air flows appeared over the central TIO (65°–75°E), which enhanced the intertropical convergence zone and upward air motions, leading to more precipitation in central TIO. An analysis shows that the AO may modulate the Arabian anticyclone through two Rossby wave paths in the upper troposphere: a midlatitude (50°–60°N) path during 1979–2001 from North Atlantic southeastward to the Middle East and the neighboring Arabian Sea; and a subtropical (20°–30°N) path during 2002–2019 from North Atlantic eastward to the Middle East and Arabian Sea. Large wave activity fluxes induced by AO were concentrated along the two paths before and after 2001, and the location of the cross-equator flows depends on the location of the anticyclone. Causes of the decadal changes in the AO-associated wave trains need further investigation.

Key words: winter Arctic Oscillation, tropical Indian Ocean, precipitation, Rossby wave

Citation: Shi, Y. W., Y. Chen, and D. Y. Gong, 2021: Decadal shift in the relationship between winter Arctic Oscillation and central Indian Ocean precipitation during the early 2000s. *J. Meteor. Res.*, **35**(5), 857–867, doi: 10.1007/s13351-021-1009-y.

1. Introduction

The tropical Indian Ocean (TIO) plays a significant role in modulating regional and worldwide climate owing to its large heat and moisture storage capacities and active interaction with the atmosphere (Hastenrath et al., 1993; Schott et al., 2009). A better understanding of the drivers or triggers of the TIO atmosphere–ocean thermal and dynamic processes is vital for improving the skill of regional climate prediction. Previous studies have shown that various local and remote forcings can exert an influence on the TIO climate.

During warm El Niño–Southern Oscillation (ENSO) summer, through modulation of the Walker circulation, an anomalous divergence center over the low-level equatorial western Pacific and an anomalous convergence center over the western tropical Indian Ocean are induced, which is complemented by anomalous divergence and subsidence over the Indian region, resulting in reduced regional rainfall (Kumar et al., 1999; Ashok et al., 2004). Klein et al. (1999) suggested that over the eastern Indian Ocean, the enhanced subsidence during El

Supported by the National Natural Science Foundation of China (41775068 and 41375071).

*Corresponding author: gdy@bnu.edu.cn

© The Chinese Meteorological Society and Springer-Verlag Berlin Heidelberg 2021

Niño reduces cloud cover and increases the solar radiation absorbed by the ocean, resulting in warmer sea surface temperature (SST). Based on a case study of the 1997/98 El Niño event, Ueda and Matsumoto (2000) reported that the change in Walker circulation related to El Niño-induced easterly wind anomalies over the equatorial Indian Ocean weakened (accelerated) the westerly (easterly) summer monsoon winds over the western (eastern) Indian Ocean. The anomalous easterlies resulting from warm ENSO could modulate SST variability over the TIO and surrounding regions as the waves propagate westward from the eastern TIO (Xie et al., 2002). Anomalous SSTs can persist to the next year along with signals decaying. The correlation coefficient between TIO SST and ENSO during summer (June–July–August, JJA) remains strong and exceeds 0.6 over much of the TIO, with the maximum correlation (0.8) over the western TIO where the thermocline is shallow (Xie et al., 2009).

The Indian Ocean Dipole (IOD) mode, which is characterized by an east–west dipole pattern in SST anomalies, is another major mode of interannual climate variability modulating the TIO oceanic and atmospheric conditions (Saji et al., 1999; Webster et al., 1999). During the peak phase of positive IOD events, the equatorial surface wind reverses direction from westerlies to easterlies, resulting in cooler SST over the southeastern TIO and warmer SST over the western Indian Ocean. Corresponding to the local SST and atmospheric circulation anomalies, there is a positive-west–negative-east structure of precipitation over the TIO as the IOD develops in September–November (Saji and Yamagata, 2003; Annamalai and Murtugudde, 2004; Rao and Behera, 2005; Yu et al., 2005).

In addition to tropical forcing, increasing evidence has disclosed that mid–high latitude factors, such as the Arctic Oscillation (AO)/North Atlantic Oscillation (NAO), can also modify the Indian Ocean and adjoining regional climates on various timescales ranging from intraseasonal to interannual. For example, on the intraseasonal timescale, observations show significant links between the AO/NAO and Madden–Julian Oscillation (MJO) (Zhou and Miller, 2005; Lin et al., 2009). By a simulation study, Lin and Brunet (2011) found that the MJO forecast skill is significantly enhanced by a strong NAO in the initial condition, with a lead time of approximately 10–25 days. On the interannual timescale, the teleconnection between the AO/NAO and Indian climate has been reported time after time. For example, Yadav et al. (2009) showed that during the positive phase of AO/NAO, the pressure gradient between the extratropical and polar North Atlantic increases, which intensifies the Asian westerly jet stream over North Africa and the Middle East, leading to more precipitation over northwestern India. Goswami et al. (2006) found that a positive NAO may cause above-normal Indian summer monsoon rainfall by strengthening the meridional gradient of tropospheric temperature over Eurasia. Kar and Rana (2014) reported that winter precipitation over northwestern India and neighboring regions tends to increase during positive AO/NAO and warm ENSO conditions. Concerning the AO/NAO and regional climate teleconnections, atmospheric Rossby waves play a key role. Intensive Rossby wave trains have been seen during positive AO years, which trigger positive geopotential heights over northwestern India and further result in excessive precipitation during the Indian winter monsoon over the northern Indian and adjoining regions (Midhuna and Dimri, 2019). Gong et al. (2013, 2014) reported that during positive AO/NAO winters, stronger downward air motion over the northern Indian Ocean and neighboring lands enhances the Arabian high, which brings stronger northeasterly winds and consequent cross-equator air flows, and the resultant more-than-normal precipitation is significant in the central TIO. The anomalous wind stress triggers oceanic Rossby waves over the southern TIO in winter, which causes anomalous SSTs and air–sea heat fluxes in summer as Rossby waves arrive in the western TIO (Gong et al., 2017a, b).

Although the AO exists in all seasons, it is most active in boreal winter (January–February–March, JFM) (Thompson and Wallace, 1998, 2000). In this study, we aim to address the issue of whether the interannual relationship between the winter AO and TIO climate is stable over time. The remainder of the paper is organized as follows. Section 2 describes the datasets and analytical methods. Section 3 presents the statistical relationship between the boreal winter AO and precipitation over the TIO for 1979–2019, focusing on the temporal features of their linkage. Comparisons of the AO-related atmospheric circulation anomalies in the lower and upper troposphere for two sub time periods of 1979–2019 are carried out in Section 4. Finally, the results are summarized and discussed in Section 5.

2. Datasets and methods

In the present study, we utilized the monthly AO index for 1979–2019, which is defined by projecting the 1000-hPa height anomalies poleward of 20°N onto the

loading spatial pattern of the AO, obtained from the Climate Prediction Center (CPC), NOAA (https://www.cpc.ncep.noaa.gov/products/precip/CWlink/daily_ao_index/ao.shtml). Because the AO pattern develops most actively during boreal winter (JFM) among all seasons (Thompson and Wallace, 1998), we confine our analysis to JFM.

We employed two SST indices including the Niño3.4 SST and IOD time series. The Niño3.4 SSTs are averaged over 5°S–5°N, 170°–120°W. The IOD is measured by an anomalous SST gradient between the western equatorial (10°S–10°N, 5°–70°E) and southeastern equatorial Indian Ocean (0–10°S, 90°–110°E) (Saji and Yamagata, 2003). In this study, monthly Niño3.4 SST and IOD time series spanning from 1979 to 2019 were obtained from NOAA's Physical Sciences Division (http://www.esrl.noaa.gov/psd/gcos_wgsp/Timeseries), and both were calculated from the HadISST1 SST fields (Rayner, 2003).

When analyzing the AO-related precipitation changes, we utilized the CPC Merged Analysis of Precipitation (CMAP; Xie and Arkin, 1997). For comparison, satellite observations of interpolated outgoing longwave radiation (OLR) data were also used to help identify robust precipitation-relevant signals (Liebmann and Smith, 1996). These climate data are available from 1979 to 2019, with a resolution of 2.5° latitude × 2.5° longitude. In addition, monthly atmospheric circulation variables from the ERA5 dataset were also utilized. The ERA5 data span from 1979 to 2019 at a spatial resolution of 1.5°.

To focus on the interannual timescale changes in the TIO climate and their relationship with AO, we applied high-pass filtering to all time series using the Butterworth filter. Only the components with timescales shorter than 10 yr were retained and employed in the following analysis. Interannual variations over the TIO are largely impacted by ENSO and the IOD, which are both characterized by strong seasonal phase locking peaking in boreal winter and fall, respectively (Rasmusson and Carpenter, 1982; Saji et al., 1999). In this study, to highlight the possible AO signals, the preceding winter Niño3.4 SST and the autumn–winter IOD signals were simply and linearly fitted to the climate variables of interest by multi-regression analysis and then removed from the original time series. This process is expected to statistically reduce/exclude their influences on the TIO. The residuals are regarded as ENSO-IOD-free parts and subjected to the subsequent analysis.

To depict the propagation of stationary Rossby waves, the two-dimensional Rossby wave activity flux (WAF) at a specific pressure level is calculated and estimated based on the following formula by Takaya and Nakamura (2001):

$$\boldsymbol{W} = \frac{1}{2\left|\overline{\boldsymbol{U}}\right|}\begin{bmatrix} \bar{u}(\psi'^2_x - \psi'\psi'_{xx}) + \bar{v}(\psi'_x\psi'_y - \psi'\psi'_{xy}) \\ \bar{u}(\psi'_x\psi'_y - \psi'\psi'_{xy}) + \bar{v}(\psi'^2_y - \psi'\psi'_{yy}) \end{bmatrix}, \quad (1)$$

where $\boldsymbol{W}$ is the horizontal component of the WAF, and an overbar and a prime represent the climatological mean and anomaly, respectively; ψ serves to illustrate the stream function; and $\boldsymbol{U} = (u, v)$ represents the horizontal wind.

3. Decadal shift in the relationship between the AO and TIO precipitation

We first investigated the JFM Indian Ocean precipitation–AO relationship during the whole data period of 1979–2019. For the sake of comparison, we used the CMAP precipitation dataset, which is the same as that used by Gong et al. (2014). In addition, we analyzed the OLR anomalies in association with the JFM AO. After the linear components of ENSO and IOD signals in the interannual time series of CMAP precipitation and OLR were estimated and excluded, we regressed the ENSO- and IOD-free variations on the AO index. The results are shown in Fig. 1. A large variance in the predictand tends to yield a large regression coefficient, which may cover up the real strength of the correlation between the predictor and predictand. Here, we plotted the distributions of correlation coefficient as contour lines. Note that for a given degree of freedom of 40, the correlation thresholds for the 95% and 99% confidence levels are approximately ± 0.30 and ± 0.39, respectively.

As seen in Fig. 1a, the CMAP regression coefficients are generally positive over the central TIO with anomalies more than 0.4 mm day^{-1}, while a negative belt is located approximately over the eastern TIO. Negative OLR anomalies appear in the central TIO to a broader extent than CMAP precipitation, and positive anomalies appear in the eastern TIO to a smaller extent than the CMAP. Their spatial patterns are generally consistent, both suggesting more-than-normal precipitation over the central TIO during positive AO years for JFM. We note that this feature is somewhat different from that of Gong et al. (2014, Fig. 2). In their studies based on CMAP precipitation with a shorter data period of 1979–2009, the maximum precipitation anomalies over the central TIO (0–10°S, 60°–80°E) are above 1 mm day^{-1}, accompanied by the correlation with the JFM AO of above 0.4. In the present study, for the data period from 1979 to 2019,

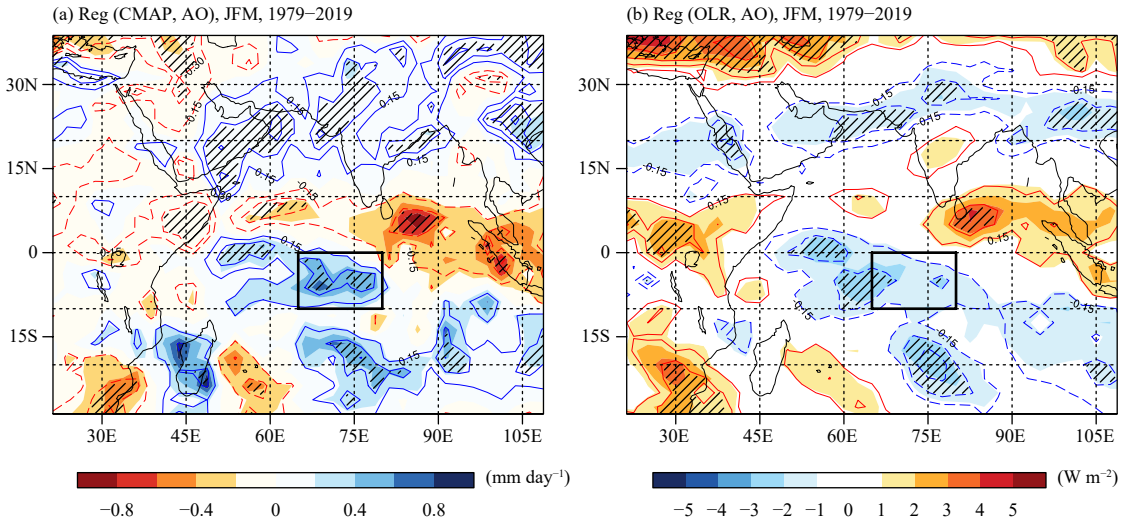

Fig. 1. Anomalies of (a) CMAP precipitation and (b) OLR in association with one-unit larger JFM AO during 1979–2019. The correlation coefficients are represented by contours. Hatched shadings denote values significant at the 95% confidence level.

the maximum precipitation anomalies over the central TIO are 0.71 mm day^{-1}, while the maximum correlation coefficient is 0.42. The AO-related changes in precipitation over the central TIO become weaker. Another apparent difference is the enhanced precipitation anomalies over 15°–30°S, 65°–75°E in 1979–2019. These results are indicative of the possible changes in the AO–precipitation relationship over time.

To reveal the details, we further investigated the temporal features of the JFM AO–precipitation correlation. Here, both the regional mean CMAP precipitation and OLR averaged over the central TIO (0–10°S, 65°–80°E) are considered (Fig. 1). After the ENSO- and IOD-related variations are linearly removed, the temporal features are shown in Fig. 2. In the filtered time series, we found that their relationships are in a good phase in the 1990s and the early 2000s but out of phase since 2009. An unstable relationship can also be found in the original unfiltered time series (Fig. 2b). To analyze the unstable features of the relationship between AO and central TIO precipitation, we computed their sliding correlation from 1979 to 2019. Here, the length of the sliding window used is 19 yr. As seen in Fig. 3, for both CMAP and OLR, their sliding correlation coefficients vary distinctly with time from 1979 to 2019. The variations are very similar for CMAP and OLR. The CMAP correlation is approximately 0.5 during 1988–1991 and displays a pronounced increase after 1992, reaching 0.7 in 1995. Afterwards, the sliding correlation decreased from 0.75 to nearly 0.4 in 2001–2002 and decreased to below 0.2 in 2008. We also investigated different sliding window lengths of 15, 17, 21, and 23 yr (figures omitted) to test

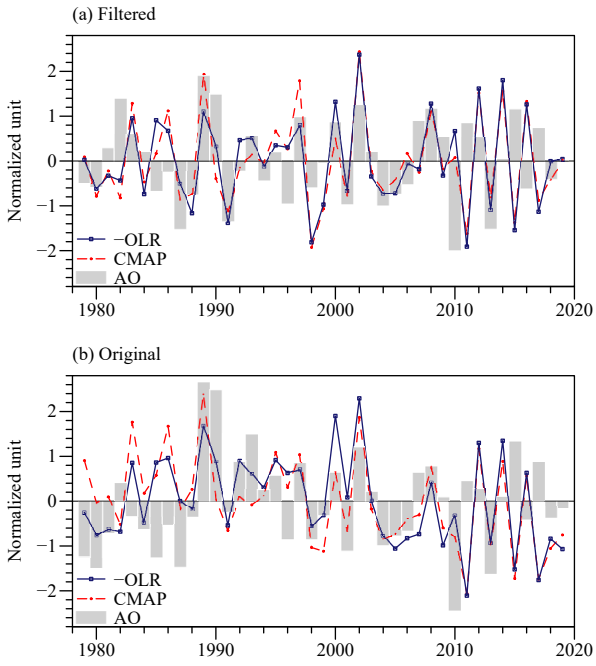

Fig. 2. Time series of (a) high-pass filtered AO, OLR, and CMAP precipitation, and (b) their original values (shown for comparison). Precipitation and OLR are averaged over the central TIO (0–10°S, 65°–80°E). The data period is 1979–2019. The OLR is multiplied by −1 to facilitate comparison.

the sensitivity of the corrections. We found that although the correlation value in a specific year varied depending upon the length of the window, the periods of high and low correlations were similar. Therefore, concerning the AO–precipitation relationship, it seems reasonable to split the total data period into two subperiods: a high correlation period from 1979 to approximately 2001 and a

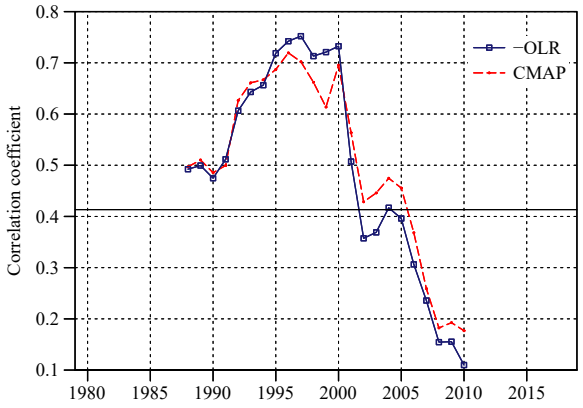

Fig. 3. Evolution of 19-yr sliding correlation coefficients between the JFM AO index and CMAP precipitation (red) and OLR (blue) from 1979 to 2019. Precipitation and OLR are averaged over the central TIO (0–10°S, 65°–80°E). The horizontal line denotes the 95% confidence level. The OLR is multiplied by −1 to facilitate comparison.

low correlation period from 2002 to 2019.

An issue arising is that the spatial patterns in the AO-related precipitation anomalies might have been different in the two subperiods. We examined the JFM CMAP precipitation and OLR changes for 1979–2001 and 2002–2019 in Fig. 4. During 1979–2001, positive precipitation anomalies over the central TIO are outstanding, where the maximum anomalies are larger than 0.95 mm day^{-1}; in addition, the maximum correlation coefficient is 0.58. In contrast, during 2002–2019, the precipitation anomalies in the same region are not significant and are less than 0.42 mm day^{-1}. A consistently weakening correlation is also seen in OLR. During 1979–2001, negative OLR anomalies dominated the central TIO, where the negative departures were lower than −3 W m^{-2}. The OLR anomalies were no longer evident during 2002–2019. We noted that over the southern Bay of Bengal, the less-than-normal precipitation remained generally unchanged in the anomalous location, as well as in magnitude, from the sliding correlation results (figure omitted). In addition, in the western TIO, the weak correlation in 1979–2001 became strongly negative in 2002–2019, particularly in the southern Arabian Sea and neighboring eastern Africa. These results suggest that the temporal changes in the AO–precipitation correlation appear not as a local phenomenon but with a salient large-scale pattern, particularly over the western–central tropical Indian Ocean. We noted that the AO–precipitation correlation became much weaker after 2010. Does this indicate a significantly different AO–precipitation relationship after 2010? We further tested the AO-related precipitation and circulation in 2010–2019 and found that the spatial features were similar to those in 2002–2019.

4. Atmospheric circulation changes

4.1 *The anomalous anticyclone over the Arabian Sea*

As analyzed above, there was a decadal shift in the AO–precipitation correlation over the central TIO in the early 2000s. Abnormal precipitation was closely related to atmospheric circulation. A question arises regarding the AO-related atmospheric circulation anomalies corresponding to precipitation anomalies. An anomalous anticyclone over the Arabian Sea was found from the surface to the upper troposphere (figures omitted). In Fig. 5, we computed the regressions of horizontal winds at 500 hPa based on the JFM AO index. To help understand the jet stream and associated wave activity, we also show the climate means of the zonal wind at 200 hPa in Fig. 4e.

As shown in Fig. 5, the salient features were large anticyclonic anomalies over the Arabian Sea just south of the Middle East jet stream during both periods. Evidently, the center locations look different in the two periods. In the early period, the anomalous center was located at approximately 14°N, 60°E, while the center moved northwestward to approximately 17°N, 56°E in 2002–2019. In addition, their intensities were virtually different.

To reveal more details, we quantitatively measured the anticyclone intensity by computing the regional mean vorticity. The AO-related anticyclonic anomalies were similar from the lower troposphere to the upper troposphere, where averaging was made from 700 to 200 hPa. Given the northwestward shift of the center location, the regions for averaging were confined within 9°–19°N, 50°–70°E for 1979–2001 and within 12°–22°N, 46°–66°E for 2002–2019. The out-of-phase covariation between the AO and vorticity was evident for both periods. The maxima of vorticity observed in 1985, 1987, 2010, and 2018 corresponded well to negative AO indices, while the minima in 1982, 1989, 2007, 2012, and 2017 were consistent with positive AO anomalies (Fig. 6). It is interesting to note that their correlation coefficients are significantly different. During the early period, the vorticity was significantly correlated with the AO index at −0.38. After 2002, their correlation became much stronger, at −0.63.

In summary, the anomalous anticyclone over the Arabian Sea moved northwestward and strengthened during 2002–2019. Over the tropics, the atmospheric response to diabatic heating (cooling) plays an important role in generating circulation anomalies (Gill 1980; Taschetto et al., 2011). In association with anomalous diabatic heating over the tropical IO caused by more-than-normal precip-

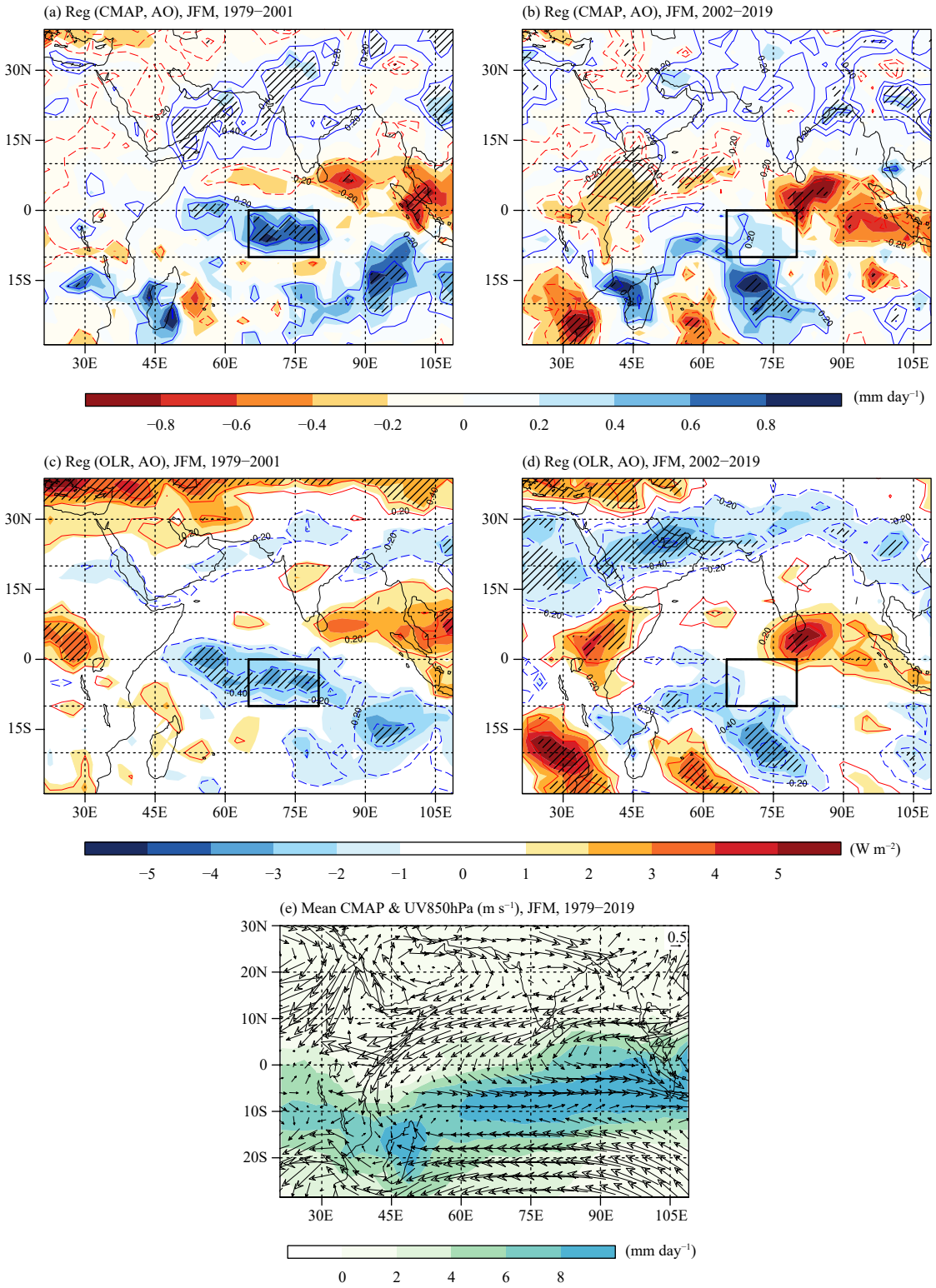

Fig. 4. Anomalies of (a, b) CMAP precipitation and (c, d) OLR corresponding to one-unit larger JFM AO during 1979–2001 and 2002–2019. The regression correlation coefficients are represented by color contours. All hatched shadings denote values at the 95% confidence level. (e) Climate means of JFM precipitation (shading) and 850-hPa horizontal winds (vector) during 1979–2019.

itation during 1979–2001, we would expect a Gill-type response of anticyclones in the upper troposphere and cyclones at the lower level over the Arabian Sea, and vice versa. However, an anomalous anticyclone over the Arabian Sea is found throughout the troposphere (figures omitted). This implies that atmospheric anomalies

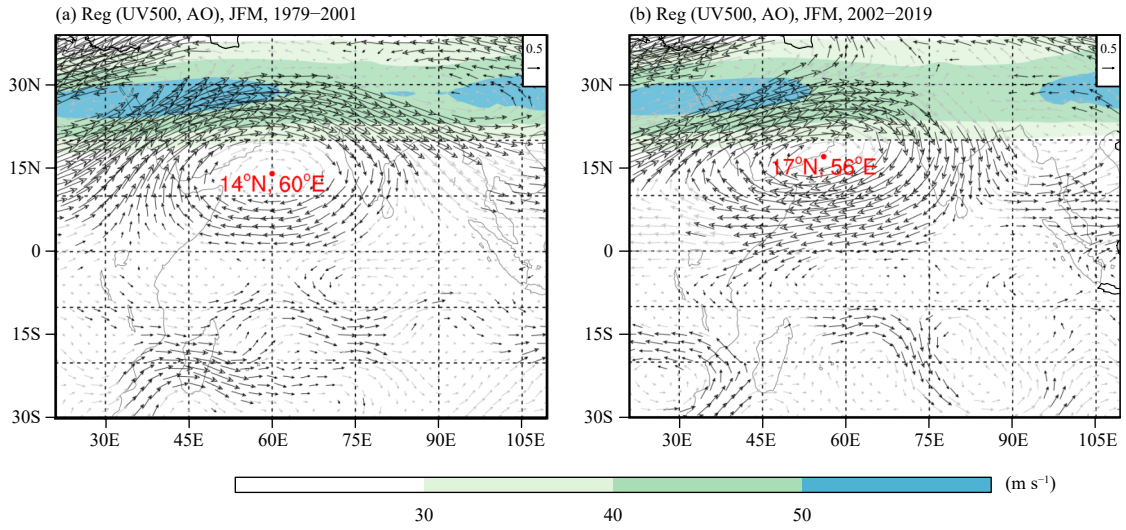

Fig. 5. Anomalous JFM horizontal winds (vector) at 500 hPa corresponding to one-unit larger JFM AO index during (a) 1979–2001 and (b) 2002–2019. The long-term mean 200-hPa zonal wind speed for the two periods are plotted in color shadings. The black vectors denote the wind anomalies that are significant at the 90% confidence level.

play the dominant role and that the possible Gill-type response for the atmosphere is somewhat weak and hard to distinguish.

Another apparent difference arises from the cross-equator air flow. As seen in Fig. 5, there were significant southward cross-equator flows between approximately 65° and 75°E during 1979–2001. The anomalous air flow could enhance the intertropical convergence zone (ITCZ) in the Southern Hemisphere, accompanied by enhanced upward air motions. These tend to result in more precipitation over the central TIO (Fig. 4). In contrast, evident cross-equator air flows were only observed in the western TIO (40°–50°E) during 2002–2019. This implies that the location of the cross-equator flows depends on the location of the anticyclone. Moreover, during 2002–2019, precipitation over the central TIO did not increase significantly as the anomalous cross-equator air flows migrated westward to 40°–50°E over the western edge of the ITCZ. Climatologically, the ITCZ spans from Madagascar eastward and strides over approximately 20°–5°S, dominant in the eastern TIO (Fig. 4e).

To explore the effects of the AO-related southward cross-equator air flow and vertical motion on the precipitation anomalies, we further investigated the regional mean meridional winds (v) at 500 hPa and the vertical velocity (ω) over 0–10°S, 65°–80°E. The regional mean vertical velocity was then vertically averaged from 925 to 300 hPa. Similar to precipitation, we computed the sliding correlations between the JFM AO and meridional winds, as well as the vertical velocity, using a 19-yr window. As shown in Fig. 7, the sliding correlation coefficients between the AO indices and meridional winds

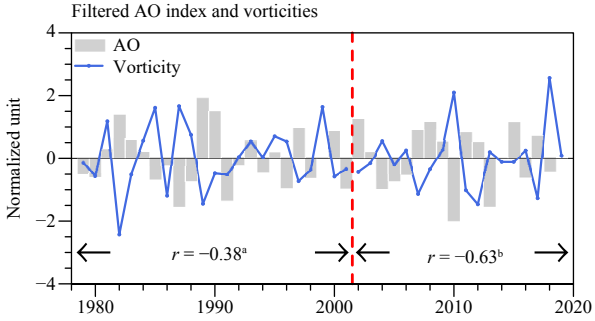

Fig. 6. Time series of the regional mean Arabian Sea vorticity and the AO index for JFM. Vorticities are regional means averaged over 9°–19°N, 50°–70°E during 1979–2001 and over 12°–22°N, 46°–66°E during 2002–2019. The superscripts a and b indicate values significant at the 90% and 99% confidence levels, respectively.

were between approximately −0.2 and −0.6 before the early 2000s. In particular, significant southerly winds were observed during 1992–2000. Similarly, the significant AO–vertical velocity correlation coefficients varied between −0.45 and −0.6 during 1979–2000. The correlations of AO with both vertical velocity and meridional wind rapidly weakened after the early 2000s. These unstable temporal correlations were consistent with temporal features in AO-related CMAP precipitation and OLR anomalies in 1979–2019 (Fig. 3). Thus, over the central TIO, the intensity and/or location of the southward cross-equator winds accompanying the anomalous Arabian Sea anticyclone may modulate the precipitation anomalies during the two periods by influencing the meridional winds (i.e., cross-equator air flows) and vertical motion associated with the ITCZ.

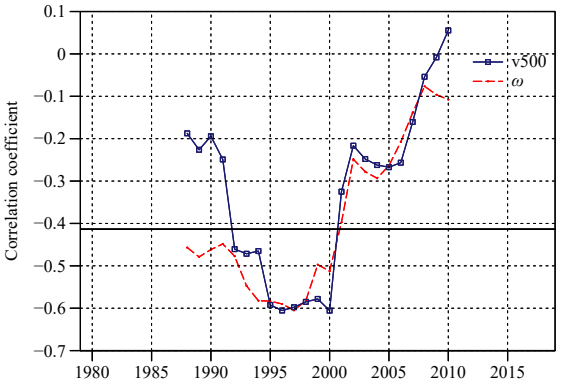

Fig. 7. Evolution of 19-yr sliding correlation coefficients between the JFM AO index and the mean vertical velocity (ω; integrated from 975 to 200 hPa) and meridional wind (v; 500 hPa; v500) averaged over the central TIO (0–10°S, 65°–80°E) from 1979 to 2019. The horizontal line denotes the 95% confidence level.

4.2 *Changes in the atmospheric wave trains*

During positive AO winter, the Rossby wave guided by westerlies emanating from the North Atlantic tends to trigger persistent positive geopotential height anomalies at the exit of the Middle East jet stream (Gong et al., 2013, 2014). A question arises as to whether the AO-related wave trains changed during 1979–2019. In this section, we compared the features of wave trains that connected the AO and regional circulation anomalies over the Arabian Peninsula during the two subperiods. We computed the anomalous meridional winds and the WAF as defined by Takaya and Nakamura (2001) at 200 hPa during the two periods (Fig. 8). To highlight the signals, we employed composites for large positive AO index years for both periods of 1979–2001 and 2002–2019. Here, positive AO years are dfined with the standardized AO index larger than 0.6. For 1979–2001, six cases were identified in 1989, 1990, 1992, 1993, 1997, and 2000. Similarly, for 2002–2019, five positive AO years were identified, i.e., 2002, 2007, 2008, 2015, and 2017. The WAF for these cases was computed in Fig. 8. Evidently, in association with positive AO phases, there were two anomalous Rossby wave trains. One wave train was located at mid–high latitudes along approximately 60°N, which propagated from the North Atlantic across the Eurasian continent. The other was located at approximately 20°N, emanating from the North Atlantic and propagating eastward downstream to the Middle East and India. By comparing the spatial features in the two subperiods, we easily found that the salient difference appears in the wave train paths. During 1979–2001, the WAF in the mid–high latitudes was relatively larger than that in 2002–2019. More importantly, the anomalous WAF that propagated from the North Atlantic to the

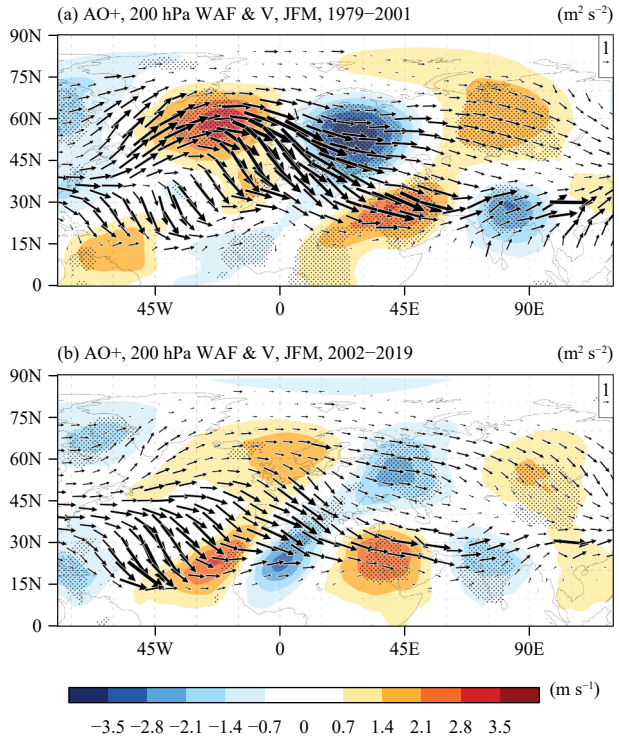

Fig. 8. Composite JFM meridional wind speed anomaly (color shaded; m s^{-1}) and wave activity flux (vector; m^2 s^{-2}) at 200 hPa for the positive AO years of (a) 1989, 1990, 1992, 1993, 1997, and 2000; and (b) 2002, 2007, 2008, 2015, and 2017. Stipples indicate values of meridional wind speed significant at the 90% confidence level.

Middle East became much weaker after 2002. The different WAFs between the two periods show a pronounced weakening of the mid–high-latitude wave train after 2002 (more figures omitted). In short, during 1979–2001, the AO-related wave trains preferred to propagate from the North Atlantic/Europe to the northern Arabian Sea; while during 2002–2019, the wave activities tended to propagate along a subtropical path from North Atlantic toward the Arabian Sea, modulating regional northeastern winds/cross-equator air flows and the precipitation over the southern ITCZ.

5. Summary and discussion

In the present study, we found that during 1979–2019, the relationship between the boreal winter AO and central TIO climate experienced an evident decadal shift in the early 2000s. There were significant correlations of approximately 0.5–0.7 between AO and precipitation over the central TIO during 1979–2001. Over the anomalous center, precipitation was as much as 0.95 mm day^{-1} in association with one-unit larger AO index, whereas negative OLR anomalies below −3 W m^{-2} were collocated consistently. In contrast, during 2002–2019, the pre-

cipitation and OLR anomalies in the central TIO were not significant.

The concurrent changes in the Arabian anticyclonic circulation in association with the AO displayed obvious differences in these two periods. During 1979–2001, the anticyclone was centered at approximately 14°N, 60°E and was relatively weak, with its correlation to AO of −0.38. However, the anticyclone center moved northwestward to approximately 17°N, 56°E and intensified, with a correlation to AO of −0.63 during 2002–2019. Correspondingly, there were significant southward cross-equator air flows and anomalous vertical air motion between approximately 65° and 75°E during 1979–2001. These tended to result in more precipitation over the central TIO. In contrast, evident cross-equator air flows were observed only at 40°–50°E during 2002–2019.

The anomalous regional circulation over the Arabian Sea and neighboring areas was tightly linked to the AO through wave trains. During 1979–2001, wave activities preferred a midlatitude path, with enhanced wave activity flux propagating from the North Atlantic southeastward to the Middle East. During 2002–2019, however, the salient feature was that the wave trains tended to propagate along with the subtropical jets from the North Atlantic eastward downstream to the Middle East. The difference in the wave activities was likely responsible for the changes in Arabian anticyclone intensity and location.

It is worth noting that during 2002–2019, the anomalous Arabian anticyclone moved northwestward and intensified. An interesting issue is whether these circulation changes influenced precipitation over the western TIO and neighboring regions. As shown in Fig. 4, significant negative precipitation and positive OLR anomalies could be found over eastern Africa in 10°S–10°N, 30°–45°E during 2002–2019, whereas precipitation and OLR anomalies there were nearly zero during 1979–2001. The temporal shifting could also be identified by the sliding correlations between the AO and regional mean CMAP and OLR over 10°S–10°N, 35°–45°E (Fig. 9). Before 2001, the correlations for both CMAP and OLR were between 0 and −0.4 and not significant; in contrast, during 2002–2019, all correlations were between −0.4 and −0.6 and significant at the 95% confidence level. It is clear that the reduction in precipitation over eastern Africa and the neighboring western TIO is consistent with the enhanced anticyclonic circulation in 2002–2019.

Another important issue is what is responsible for the decadal changes in the AO-related wave trains. There are some potential clues. First, the dynamic features of the

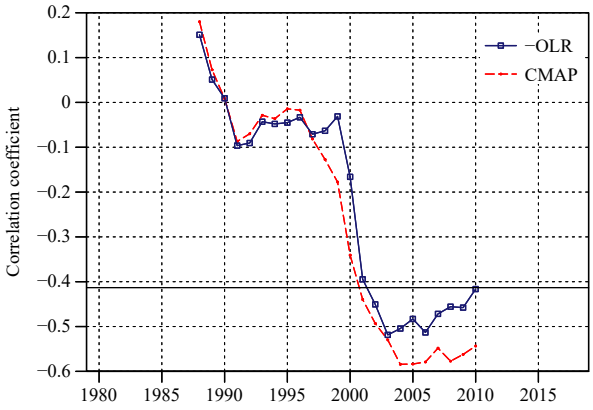

Fig. 9. Evolution of 19-yr sliding correlation coefficients between the JFM AO index and CMAP precipitation and OLR from 1979 to 2019. Precipitation and OLR are averaged over eastern Africa (10°S–10°N, 35°–45°E). The horizontal line denotes the 95% confidence level. The OLR is multiplied by −1 to facilitate comparison.

AO experienced low-frequency changes. For example, the extent of the NAO/AO-related pressure centers over the North Atlantic and North Pacific decreased after the middle 1990s (Overland and Wang, 2005; Zhao et al., 2010). It is unclear whether wave sources and activity could change and correspondingly alter regional atmospheric circulation over the Middle East and Arabian Sea. Second, it is well recognized that SST anomalies in the North Atlantic play an important role in modulating the atmospheric circulation over downstream regions on the interannual timescale (Rajeevan and Sridhar, 2008; Lim, 2015; Lu et al., 2020). The AO-related circulation anomalies may be modulated by decadal changes in SSTs, such as the transition from a negative SST phase to a warmer condition occurring in the late 1990s (Knight et al., 2005; Goswami et al., 2006). However, this issue has not been well addressed. Third, the AO-related wave activities may depend on the configuration of the westerlies. Previous studies have reported that since 1979, the subtropical jet stream has changed with regard to its speed (Pena-Ortiz et al., 2013; Manney and Hegglin, 2018) and location (Grise et al., 2018; Manney and Hegglin, 2018; Staten et al., 2018) and has meandered (Francis and Vavrus, 2015; Di Capua and Coumou, 2016). Note that Rossby wave activities are sensitive to these westerly dynamic features (Hoskins and Ambrizzi, 1993; Branstator, 2002; Branstator and Teng, 2017). As shown in Fig. 5, the jets over northern Africa to the Middle East displayed evident differences in strength and location during 1979–2001 and 2002–2019, implying that the decadal change in jet streams might have played a role in modulating AO-related wave trains. All these possible mechanisms require further substantial analyses.

Acknowledgments. The ERA5 reanalysis data used in this study were obtained from ECMWF at http://www.ecmwf.int/. The CMAP precipitation and interpolated OLR data were provided by the NOAA/OAR/ESRL PSD, Boulder, Colorado, USA, from their website at http://www.esrl.noaa.gov/psd.

REFERENCES

Annamalai, H., and R. Murtugudde, 2004: Role of the Indian Ocean in regional climate variability. *Earth's Climate*: *The Ocean–Atmosphere Interaction*, C. Wang, S. P. Xie, and J. A. Carton, Eds., American Geophysical Union, Washington, 213–246.

Ashok, K., Z. Y. Guan, N. H. Saji, et al., 2004: Individual and combined influences of ENSO and the Indian Ocean dipole on the Indian summer monsoon. *J. Climate*, **17**, 3141–3155, doi: 10.1175/1520-0442(2004)017<3141:IACIOE>2.0.CO;2.

Branstator, G., 2002: Circumglobal teleconnections, the jet stream waveguide, and the North Atlantic Oscillation. *J. Climate*, **15**, 1893–1910, doi: 10.1175/1520-0442(2002)015<1893:CTTJSW>2.0.CO;2.

Branstator, G., and H. Y. Teng, 2017: Tropospheric waveguide teleconnections and their seasonality. *J. Atmos. Sci.*, **74**, 1513–1532, doi: 10.1175/JAS-D-16-0305.1.

Di Capua, G., and D. Coumou, 2016: Changes in meandering of the Northern Hemisphere circulation. *Environ. Res. Lett.*, **11**, 094028, doi: 10.1088/1748-9326/11/9/094028.

Francis, J. A., and S. J. Vavrus, 2015: Evidence for a wavier jet stream in response to rapid Arctic warming. *Environ. Res. Lett.*, **10**, 014005, doi: 10.1088/1748-9326/10/1/014005.

Gill, A. E., 1980: Some simple solutions for heat-induced tropical circulation. *Quart. J. Roy. Meteor. Soc.*, **106**, 447–462, doi: 10.1002/qj.49710644905.

Gong, D. Y., Y. Q. Gao, M. Hu, et al., 2013: Association of Indian ocean ITCZ variations with the Arctic Oscillation during boreal winter. *Atmos. Ocean. Sci. Lett.*, **6**, 300–305, doi: 10.3878/j.issn.1674-2834.12.0108.

Gong, D. Y., Y. Q. Gao, D. Guo, et al., 2014: Interannual linkage between Arctic/North Atlantic Oscillation and tropical Indian Ocean precipitation during boreal winter. *Climate Dyn.*, **42**, 1007–1027, doi: 10.1007/s00382-013-1681-4.

Gong, D. Y., D. Guo, Y. Q. Gao, et al., 2017a: Boreal winter Arctic Oscillation as an indicator of summer SST anomalies over the western tropical Indian Ocean. *Climate Dyn.*, **48**, 2471–2488, doi: 10.1007/s00382-016-3216-2.

Gong, D. Y., D. Guo, S. Li, et al., 2017b: Winter AO/NAO modifies summer ocean heat content and monsoonal circulation over the western Indian Ocean. *J. Meteor. Res.*, **31**, 94–106, doi: 10.1007/s13351-017-6175-6.

Goswami, B. N., M. S. Madhusoodanan, C. P. Neema, et al., 2006: A physical mechanism for North Atlantic SST influence on the Indian summer monsoon. *Geophys. Res. Lett.*, **33**, L02706, doi: 10.1029/2005GL024803.

Grise, K. M., S. M. Davis, P. W. Staten, et al., 2018: Regional and seasonal characteristics of the recent expansion of the tropics. *J. Climate*, **31**, 6839–6856, doi: 10.1175/JCLI-D-18-0060.1.

Hastenrath, S., A. Nicklis, and L. Greischar, 1993: Atmospheric–hydrospheric mechanisms of climate anomalies in the western equatorial Indian Ocean. *J. Geophys. Res. Oceans*, **98**, 20219–20235, doi: 10.1029/93JC02330.

Hoskins, B. J., and T. Ambrizzi, 1993: Rossby wave propagation on a realistic longitudinally varying flow. *J. Atmos. Sci.*, **50**, 1661–1671, doi: 10.1175/1520-0469(1993)050<1661:RWPOAR>2.0.CO;2.

Kar, S. C., and S. Rana, 2014: Interannual variability of winter precipitation over Northwest India and adjoining region: Impact of global forcings. *Theor. Appl. Climatol.*, **116**, 609–623, doi: 10.1007/s00704-013-0968-z.

Klein, S. A., B. J. Soden, and N. C. Lau, 1999: Remote sea surface temperature variations during ENSO: Evidence for a tropical atmospheric bridge. *J. Climate*, **12**, 917–932, doi: 10.1175/1520-0442(1999)012<0917:RSSTVD>2.0.CO;2.

Knight, J. R., R. J. Allan, C. K. Folland, et al., 2005: A signature of persistent natural thermohaline circulation cycles in observed climate. *Geophys. Res. Lett.*, **32**, L20708, doi: 10.1029/2005GL024233.

Kumar, K. K., B. Rajagopalan, and M. A. Cane, 1999: On the weakening relationship between the Indian Monsoon and ENSO. *Science*, **284**, 2156–2159, doi: 10.1126/science.284.5423.2156.

Liebmann, B., and C. A. Smith, 1996: Description of a complete (interpolated) outgoing longwave radiation dataset. *Bull. Amer. Meteor. Soc.*, **77**, 1275–1277, doi: 10.1175/1520-0477-77.6.1274.

Lim, Y. K., 2015: The East Atlantic/West Russia (EA/WR) teleconnection in the North Atlantic: Climate impact and relation to Rossby wave propagation. *Climate Dyn.*, **44**, 3211–3222, doi: 10.1007/s00382-014-2381-4.

Lin, H., and G. Brunet, 2011: Impact of the North Atlantic Oscillation on the forecast skill of the Madden–Julian Oscillation. *Geophys. Res. Lett.*, **38**, L02802, doi: 10.1029/2010GL046131.

Lin, H., G. Brunet, and J. Derome, 2009: An observed connection between the North Atlantic Oscillation and the Madden–Julian Oscillation. *J. Climate*, **22**, 364–380, doi: 10.1175/2008JCLI2515.1.

Lu, R., Z. W. Zhu, T. Li, et al., 2020: Interannual and interdecadal variabilities of spring rainfall over Northeast China and their associated sea surface temperature anomaly forcings. *J. Climate*, **33**, 1423–1435, doi: 10.1175/JCLI-D-19-0302.1.

Manney, G. L., and M. I. Hegglin, 2018: Seasonal and regional variations of long-term changes in upper-tropospheric jets from reanalyses. *J. Climate*, **31**, 423–448, doi: 10.1175/JCLI-D-17-0303.1.

Midhuna, T. M., and A. P. Dimri, 2019: Impact of Arctic Oscillation on Indian winter monsoon. *Meteor. Atmos. Phys.*, **131**, 1157–1167, doi: 10.1007/s00703-018-0628-z.

Overland, J. E., and M. Wang, 2005: The Arctic climate paradox: The recent decrease of the Arctic Oscillation. *Geophys. Res. Lett.*, **32**, L06701, doi: 10.1029/2004GL021752.

Pena-Ortiz, C., D. Gallego, P. Ribera, et al., 2013: Observed trends in the global jet stream characteristics during the second half of the 20th century. *J. Geophys. Res. Atmos.*, **118**, 2702–2713, doi: 10.1002/jgrd.50305.

Rajeevan, M., and L. Sridhar, 2008: Inter-annual relationship between Atlantic sea surface temperature anomalies and Indian summer monsoon. *Geophys. Res. Lett.*, **35**, L21704, doi: 10.

1029/2008GL036025.

Rao, S. A., and S. K. Behera, 2005: Subsurface influence on SST in the tropical Indian Ocean: Structure and interannual variability. *Dyn. Atmos. Oceans*, **39**, 103–135, doi: 10.1016/j.dynatmoce.2004.10.014.

Rasmusson, E. M., and T. H. Carpenter, 1982: Variations in tropical sea surface temperature and surface wind fields associated with the Southern Oscillation/El Niño. *Mon. Wea. Rev.*, **110**, 354–384, doi: 10.1175/1520-0493(1982)110<0354:VITSST>2.0.CO;2.

Rayner, N. A., D. E. Parker, E. B. Horton, et al., 2003: Global analyses of sea surface temperature, sea ice, and night marine air temperature since the late nineteenth century. *J. Geophys. Res. Atmos.*, **108**, 4407, doi: 10.1029/2002JD002670.

Saji, N. H., B. N. Goswami, P. N. Vinayachandran, et al., 1999: A dipole mode in the tropical Indian Ocean. *Nature*, **401**, 360–363, doi: 10.1038/43854.

Saji, N. H., and T. Yamagata, 2003: Possible impacts of Indian Ocean Dipole mode events on global climate. *Climate Res.*, **25**, 151–169, doi: 10.3354/cr025151.

Schott, F. A., S. P. Xie, and J. P. McCreary Jr., 2009: Indian Ocean circulation and climate variability. *Rev. Geophys.*, **47**, RG1002, doi: 10.1029/2007RG000245.

Staten, P. W., J. Lu, K. M. Grise, et al., 2018: Re-examining tropical expansion. *Nat. Climate Change*, **8**, 768–775, doi: 10.1038/s41558-018-0246-2.

Takaya, K., and H. Nakamura, 2001: A formulation of a phase-independent wave-activity flux for stationary and migratory quasigeostrophic eddies on a zonally varying basic flow. *J. Atmos. Sci.*, **58**, 608–627, doi: 10.1175/1520-0469(2001)058<0608:AFOAPI>2.0.CO;2.

Taschetto, A. S., A. S. Gupta, H. H. Hendon, et al., 2011: The contribution of Indian Ocean sea surface temperature anomalies on Australian summer rainfall during El Niño events. *J. Climate*, **24**, 3734–3747, doi: 10.1175/2011JCLI3885.1.

Thompson, D. W. J., and J. M. Wallace, 1998: The Arctic oscillation signature in the wintertime geopotential height and temperature fields. *Geophys. Res. Lett.*, **25**, 1297–1300, doi: 10.1029/98GL00950.

Thompson, D. W. J., and J. M. Wallace, 2000: Annular modes in the extratropical circulation. Part I: Month-to-month variability. *J. Climate*, **13**, 1000–1016, doi: 10.1175/1520-0442(2000)013<1000:AMITEC>2.0.CO;2.

Ueda, H., and J. Matsumoto, 2000: A possible triggering process of east–west asymmetric anomalies over the Indian Ocean in relation to 1997/98 El Niño. *J. Meteor. Soc. Japan*, **78**, 803–818, doi: 10.2151/jmsj1965.78.6_803.

Webster, P. J., A. M. Moore, J. P. Loschnigg, et al., 1999: Coupled ocean–atmosphere dynamics in the Indian Ocean during 1997–98. *Nature*, **401**, 356–360, doi: 10.1038/43848.

Xie, P. P., and P. A. Arkin, 1997: Global precipitation: A 17-year monthly analysis based on gauge observations, satellite estimates, and numerical model outputs. *Bull. Amer. Meteor. Soc.*, **78**, 2539–2558, doi: 10.1175/1520-0477(1997)078<2539:GPAYMA>2.0.CO;2.

Xie, S. P., H. Annamalai, F. A. Schott, et al., 2002: Structure and mechanisms of South Indian Ocean climate variability. *J. Climate*, **15**, 864–878, doi: 10.1175/1520-0442(2002)015<0864:SAMOSI>2.0.CO;2.

Xie, S. P., K. M. Hu, J. Hafner, et al., 2009: Indian Ocean capacitor effect on Indo–Western Pacific climate during the summer following El Niño. *J. Climate*, **22**, 730–747, doi: 10.1175/2008JCLI2544.1.

Yadav, R. K., K. R. Kumar, M. Rajeevan, 2009: Increasing influence of ENSO and decreasing influence of AO/NAO in the recent decades over Northwest India winter precipitation. *J. Geophys. Res. Atmos.*, **114**, D12112, doi: 10.1029/2008JD011318.

Yu, W. D., B. Q. Xiang, L. Liu, et al., 2005: Understanding the origins of interannual thermocline variations in the tropical Indian Ocean. *Geophys. Res. Lett.*, **32**, L24706, doi: 10.1029/2005GL024327.

Zhao, J. P., Y. Cao, and J. X. Shi, 2010: Spatial variation of the Arctic Oscillation and its long-term change. *Tellus A Dyn. Meteor. Oceanogr.*, **62**, 661–672, doi: 10.1111/j.1600-0870.2010.00472.x.

Zhou, S. T., and A. J. Miller, 2005: The interaction of the Madden–Julian Oscillation and the Arctic Oscillation. *J. Climate*, **18**, 143–159, doi: 10.1175/JCLI3251.1.

Tech & Copy Editor: Mengyuan CHEN